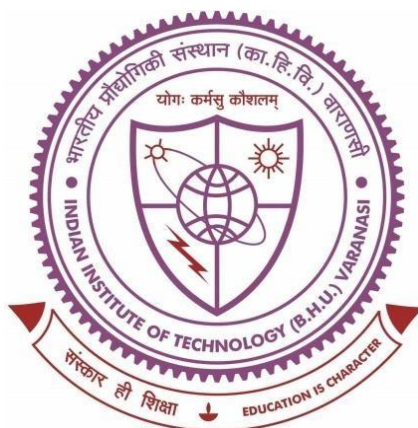


**Conformational landscape and metal-molecule
interaction of diverse molecular systems:
Insights from *ab initio* electronic structure
calculations**



**THESIS SUBMITTED IN PARTIAL FULFILLMENT
FOR THE AWARD OF DEGREE**

DOCTOR OF PHILOSOPHY

By

POONAM BHADORIA

**Department of Chemistry
Indian Institute of Technology
(Banaras Hindu University), Varanasi**

Roll No. 18051001

Year 2023

*Dedicated to
My brother (Late W.O. Mahavir Singh Bhadoria) and
My parents (Smt. Pushpa and Shri Vishwanath singh Bhadoria)*

CERTIFICATE

It is certified that the work contained in the thesis titled "**Conformational landscape and metal-molecule interaction of diverse molecular systems: Insights from *ab initio* electronic structure calculations**" by **POONAM BHADORIA** has been carried out under my supervision and that this work has not been submitted elsewhere for a degree.

It is further certified that the student has fulfilled all the requirements of Comprehensive Examination, Candidacy and SOTA for the award of Ph.D. Degree.



Dr. V. Ramanathan
(Supervisor)

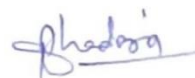
Department of chemistry
Indian Institute of Technology
(BHU), Varanasi-221005, India

DECLARATION BY THE CANDIDATE

I, **POONAM BHADORIA**, certify that the work embodied in this thesis is my own *bona-fide* work and carried out by me under the supervision of **Dr. V. Ramanathan** from **July, 2018** to **September, 2023** at the **Department of Chemistry**, Indian Institute of Technology (BHU) Varanasi. The matter embodied in this thesis has not been submitted for the award of any other degree/diploma. I declare that I have faithfully acknowledged and given credits to the research workers wherever their works have been cited in my work in this thesis. I further declare that I have not willfully copied any other's work, paragraphs, text, data, results, etc., reported in journals, books, magazines, reports dissertations, theses, etc., or available at websites and have not included them in this thesis and have not cited as my own work.

Date: 22/09/2023

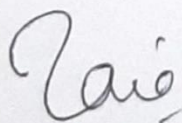
Place: VARANASI, U.P.



(POONAM BHADORIA)

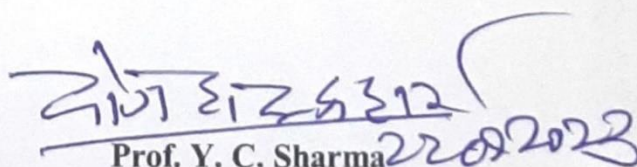
CERTIFICATE BY THE SUPERVISOR

It is certified that the above statement made by the student is correct to the best of my knowledge.



Dr. V. Ramanathan
(Supervisor)

Department of Chemistry
Indian Institute of Technology
Banaras Hindu University),
Varanasi-221005, India



Prof. Y. C. Sharma
(Head)

Department of Chemistry
Indian Institute of Technology
Banaras Hindu University),
Varanasi-221005, India

विभागाध्यक्ष / HEAD
रसायन विज्ञान विभाग
Department of Chemistry
भारतीय प्रौद्योगिकी संस्थान (का.हि.वि.वि.)
Indian Institute of Technology (B.H.U.)
वाराणसी-२२१००५ / Varanasi-221005

COPYRIGHT TRANSFER CERTIFICATE

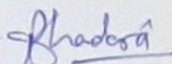
Title of the Thesis: "Conformational landscape and metal-molecule interaction of diverse molecular systems: Insights from *ab initio* electronic structure calculations"

Name of the Student: POONAM BHADORIA

COPYRIGHT TRANSFER

The undersigned hereby assigns to the Institute of Technology (Banaras Hindu University) Varanasi all rights under copyright that may exist in and for the above thesis submitted for the award of the "*Doctor of Philosophy*" degree.

Date: 22/09/2023



Place: VARANASI, U.P.

(POONAM BHADORIA)

Note: However, the author may reproduce or authorize others to reproduce material extracted verbatim from the thesis or derivative of the thesis for author's personal use provided that the source and the Institute's copyright notice are indicated.

Acknowledgement

I would like to begin by expressing my gratitude to my supervisor Dr. V. Ramanathan, for the unwavering support, guidance, and enlightening discussions we shared throughout my Ph.D. journey. Beyond the realm of academia, our conversations about life's myriad facets have undoubtedly contributed to my personal growth and shaped me into a more enlightened individual. His problem-solving approach and method of addressing challenges in our research work have been invaluable lessons in cultivating a positive and scientific mindset when tackling problems. I am genuinely thankful for his role as a mentor during this transformative Ph.D. journey.

I would like to extend my gratitude to the Department of Chemistry's Head, Prof. Y. C. Sharma, along with former Heads, Prof. R. B. Rastogi and Prof. Dhanesh Tiwary. Their provision of essential research facilities within the department played a pivotal role in facilitating the successful completion of my research endeavors.

I also would like to thank to my RPEC members Prof. Indrajit Sinha (Department of Chemistry) and Dr. Sunil Kumar Mishra (Department of Physics) for their valuable suggestions during my research progress evaluation.

I am deeply grateful to Prof. D. Tiwary for generously providing me with additional laboratory space.

I would like to express my gratitude to Dr. Brijesh Kumar Mishra for his assistance in comprehending computational chemistry.

I am also grateful to all the faculty members of the Department of Chemistry at IIT (BHU), Varanasi, for their support and encouragement.

I also extend my gratitude to all the non-teaching staff in my department for their support and care.

I also want to say thank you to my labmates for helping me with my work.

I would also like to express my heartfelt gratitude to my friends, Shreyasi Majumdar, Parul Ravat, Neetu Verma, Neha Jatav, and Siddhi Jaiswal for their unwavering presence and for crafting cherished and unforgettable moments of joy during my PHD.

I would also like to extend my thanks to my seniors, Manish, Suresh, Nivedita and Alok, for their support and kind demeanor towards me.

I am grateful to acknowledge the Indian Institute of Technology (BHU), Varanasi, for the infrastructural (Central Instrumentation facility, PARAM SHIVAY supercomputer and

Computational cluster) support and fellowship.

I can't express how fortunate I am to have you, Mamma and Papa, as my parents. Thank you for always being there for me. I truly don't need any other friends because I have both of you as my friends as well. All I can say is that I wish to have you both as my parents in all my future lifetimes, if I ever have the opportunity to be reborn on this planet Earth.

I am immensely grateful to all my siblings, including Anshu, Madan, and Neha, for their unwavering support and their patience in tolerating me.

I am also grateful to my niece, Annie, for her inspiring presence.

In the tapestry of my life, there exists a figure of profound importance, someone whom I've never encountered an equal to, and that person is my "Bhaiya." I find myself at a loss for words to convey the depth of my gratitude for your unwavering support, your unwavering help, and your constant presence in my journey. It is thanks to you that I am on the path to becoming a doctor, earning my Ph.D. Your contributions are immeasurable, and my gratitude knows no bounds.

I would also like to express my gratitude to my grandparents, who have always showered me with their blessings and affection.

Last but certainly not least, I wish to offer my gratitude to the divine, to Mahadev, my God. It's challenging to pinpoint a specific reason to thank you, for my very existence is a testament to your grace. Please continue to guide me and remain with me, both during this lifetime and beyond.

---- POONAM BHADORIA

CONTENTS

Abbreviations	XIII-XIV
List of symbols	XV-XVI
List of Figures	XVII -XXI
List of Tables	XXII- XXVI
Preface	XXVII-XXIX
CHAPTER-1	1-39
1. Introduction	1
1.1 Conformational Analysis	1-3
1.2 Non-covalent interaction	3
1.2.1 Types of non-covalent interactions/H-bonding interactions	3-4
1.2.2 H-Bonding	4-6
1.2.3 Sulfur centered H-bonding (SCHBs) [Unconventional/non-classical]	6-7
1.3 Molecule-metal cluster Interaction	7-8
1.4 Computational methods	8-20
1.4.1 Born-Oppenheimer Approximation	8-9
1.4.2 Density functional theory	9
1.4.2.1 Hohenberg-Kohn Theorems	9-10
1.4.2.2 Kohn-Sham Equation	10-12
1.4.2.3 Exchange Correlation Energy	12
1.4.3 Møller-Plesset Perturbation Theory	12-15
1.4.4 Coupled cluster (CC) methods	15-17
1.4.5 Basis Set	17-18
1.4.6 Complete basis set (CBS) limit extrapolation	18-19
1.4.7 Computation of Interaction Energy (IE)	19
1.4.7.1 Basis set superposition error (BSSE) Correction	19-20
1.5 Computational tools	20
1.6 Molecular Properties	20-27
1.6.1 Optimization of geometry	20
1.6.1.1 Dihedral relaxed scan	21

1.6.2 Analysis of vibrational modes	21-22
1.6.3 Natural Bond Orbital (NBO) calculation	22-23
1.6.4 Quantum theory of atoms in molecules (QTAIM)	23-24
1.6.5 Non-Covalent Interaction (NCI) Plot	24-25
1.6.6 Frontier molecular orbital (FMO) Analysis	25-26
1.6.7 Charge Analysis	26-28
1.6.7.1 Hirshfeld Charge	26-27
1.6.7.2 Merz Kollman (MK) ESP charge and ESP (Electrostatic potential) surface plot	27-28
1.7 Objective of Thesis	28
1.8 References	29-39
CHAPTER-2	40-108
2.1 Introduction	40-42
2.2 Computational Details	43-44
2.3 Results and discussion	44-98
2.3.1a Conformational analysis of psilocybin	44-48
2.3.1b Conformational analysis of psilocin	48-53
2.3.1c Conformational analysis of mescaline	53-57
2.3.2a Geometrical analysis of psilocybin	57-59
2.3.2b Geometrical analysis of psilocin	59-60
2.3.2c Geometrical analysis of mescaline	60-62
2.3.3a FMO of psilocybin	62-63
2.3.3b FMO of psilocin	64-65
2.3.3c FMO of mescaline	65-66
2.3.4a NBO of psilocybin	67-69
2.3.4b NBO of psilocin	69-71
2.3.4c NBO of mescaline	71-74
2.3.5a AIM analysis of psilocybin	74-76
2.3.5b AIM analysis of psilocin	76-82
2.3.5c AIM analysis of mescaline	82
2.3.6 RDG analysis of mescaline	82-84
2.3.7a Charge analysis of psilocybin	84-86
2.3.7b Charge analysis of Psilocin	87-88

2.3.7c Charge analysis of mescaline	88-91
2.3.8a Electrostatic potential maps (MEPs) of psilocybin	91-92
2.3.8b Electrostatic potential maps (MEPs) of psilocin	92
2.3.8c Electrostatic potential maps (MEPs) of mescaline	93
2.3.9a Spectroscopic analysis of psilocybin	93-95
2.3.9b Spectroscopic analysis of psilocin	95-97
2.3.9c Spectroscopic analysis of mescaline	97-98
2.4 Conclusion	99-100
2.5 References	101-108
CHAPTER-3	109-141
3.1 Introduction	109-110
3.2 Computational and Experimental Details	110-111
3.3 Results and discussion	111-137
3.3.1 Conformational Analysis	111-120
3.3.2 Normal modes Analysis	120-123
3.3.3 Analysis of Intramolecular H-bond formation	123-128
3.3.4 NBO calculations	128-130
3.3.5 ESP Charge and FMO Analysis	130-137
3.4 Conclusion	137
3.5 References	137-141
CHAPTER-4	142-192
4.1 Introduction	142-143
4.2 Computational Details	143-145
4.3 Results and discussion	145-185
4.3.1 Conformational Analysis	145-159
4.3.2 LED Calculation	159-160
4.3.3 Investigation of Intra/Inter-molecular H-bond Interactions in dimers of TGA	160-163
4.3.4 Investigation of Intra/Inter-molecular H-bond Interactions in trimers of TGA	163-167
4.3.5 NBO analysis	167-173
4.3.6 Charge analysis	174-178

4.3.7 FMO analysis	178-181
4.3.8 Normal mode analysis	181-185
4.4 Conclusion	186
4.5 References	186-192
CHAPTER-5	193-212
5.1 Introduction	193-194
5.2 Computational Details	194-195
5.3 Results and discussion	195-208
5.3.1 Geometry optimization	195-198
5.3.2 Vibrational analysis	198-201
5.3.3 DOS (density of states) analysis	201-202
5.3.4 NBO analysis	202-203
5.3.5 AIM analysis	203-204
5.3.6 FMO analysis	205-206
5.3.7 Charge analysis	206-208
5.4 Conclusion	209
5.5 References	209-212
CHAPTER-6	213-234
6.1 Introduction	213-215
6.2 Computational details	215-216
6.3 Results and discussion	216-229
6.3.1 Geometry optimization and simulated SERS spectrum of PATP/DMAB on the copper cluster	216-221
6.3.2 Photon-driven charge transfer (PD-CT) excited state calculations for PATP/DMAB on copper cluster	221-222
6.3.3 Geometry optimization and simulated SERS spectrum of PATP on the bismuth oxycarbonate (BOC) cluster	222-223
6.3.4 FMO (frontier molecular orbital) analysis of PATP@BOC	224
6.3.5a TDOS (total density of states) analysis of PATP/DMAB @ Cu ₅ cluster	225-226
6.3.5b TDOS (total density of states) analysis of PATp @ BOC	226-227
6.3.6 ESP MEP of PATP/DMAB @ Cu ₅ cluster	227-229
6.4 Conclusion	230-231

6.5 References	231-234
CHAPTER-7	235-239
7.1 Summary	235-238
7.2 Future Scope	238-239
APPENDIX	240-243
LIST OF PUBLICATIONS	244

ABBREVIATIONS

IUPAC	International union of pure and applied chemistry
NC	Noncovalent
NCI	Noncovalent interaction
CHB	Conventional hydrogen bond
UHB	Unconventional hydrogen bond
SCHB	Sulfur centered hydrogen bonds
HF	Hartree-Fock
AM1	Austin Model 1
PM6	Parameterization Method 6
M06	Minnesota 06
PW91PW91	Perdew-Wang 1991 (PW91) generalized gradient approximation
LANL2DZ	Los Alamos National Laboratory 2 Double-Zeta
DFT	Density Functional Theory
TD-DFT	Time dependent density functional theory
LDA	Local density approximation
GGA	Generalized gradient approximation
BLYP	Becke Lee Yang Parr
B3LYP	Becke 3-parameter Lee Yang Parr
MP2	Møller-Plesset second order perturbation theory
CC	Coupled cluster
CCSD	Coupled cluster single double excitation
CCSD(T)	Coupled cluster single double triple excitation
IE	Interaction Energy
LED	Local energy decomposition
DOS	Density of states
TDOS	Total density of states
PDOS	Projected density of states
BSSE	Basis set super position error
ZPE	Zero-point energy correction
CBS	Complete basis set
QTAIM	Quantum theory of atoms in molecule theory

BCP	Bond Critical point
RDG	Reduced density gradient
NAOs	Natural atomic orbitals
DMOs	Delocalised molecular orbitals
NBO	Natural bond orbital
FMO	Frontier molecular orbital
HOMO	Highest occupied molecular orbital
LUMO	Lowest unoccupied molecular orbital
MK	Merz Kollman
ESP	Electrostatic potential
UV	Ultraviolet
NMR	Nuclear magnetic resonance
GIAO	Gauge-independent atomic orbital
IR	Infrared
PES	Potential energy surface
LSD	Lysergic acid diethylamide
5-HT	5-hydroxytryptamine
EC	Effective concentration
DTT	Dithiothreitol
TGA	Thioglycolic acid
BOC	Bismuthoxycarbonate
PATP	para-aminothiophenol
DMAB	Dimercaptoazobenzene
SERS	Surface-enhanced Raman Scattering

List of Symbols

Ψ	Wave function
\hat{H}	Hamiltonian operator
$\rho(\mathbf{r})$	Electron density
ρ_{BCP}	Electron density at BCP
G_{BCP}	Kinetic electron energy density
V_{BCP}	Potential electron density
$\nabla^2 \rho_{\text{BCP}}$	Laplacian electron density
H_{BCP}	Total electron density
a.u.	Arbitrary unit
ZPE	Zero point energy
E_{int}	Interaction energy
IE	Interaction energy
μ	Chemical potential
χ	Electronegativity
η	Hardness
ω	Electrophilicity index
D	Debye
kcal/mol	Kilo calorie per mole
eV	Electron volt
μ	Dipole moment
Θ	Theta
\AA	Angstrom
Φ	Phi
E(2)	Second order perturbation stabilization energy
LP	Lone pair of electron
σ	Bonding molecular orbital
σ^*	Antibonding molecular orbital
π	Pi bonding orbital
π^*	Pi antibonding orbital
ν	Stretching frequency
ν_s	Symmetric stretching
ν_{as}	Asymmetric stretching

δ	In-plane bending
δ_s	In-plane scissoring
ω	Out of plane wagging
τ	Out of plane twisting
β	Out of plane bending
ρ	In-plane rocking
γ	Out of plane bending vibration
ϕ	Scissoring vibration
α	Ring deformation
nm	Nanometer
ppm	Parts per million
amu	atomic mass unit
cm⁻¹	centimeter inverse/wavenumber

LIST OF FIGURES

Figure No.	DESCRIPTION	Page No.
1.1	Schematic representation of different types of H-bonding	5
2.1	Dihedral angle-relative energy curve (a-d) of psilocybin at B3LYP/cc-pVTZ level of theory	45
2.2	Optimized structures of Conformers A & B of psilocybin (numbers on atoms represent the label of that atom in the optimized geometry)	46
2.3	The a,b,c, and d curves are the Dihedral-relative energy curve of psilocybin molecule at B3LYP/cc-pVTZ level of theory	47
2.4	Plot of relative energy vs. methods	47
2.5	Potential energy curve [a (C15-C18 bond rotation) and b (C8-C15 bond rotation)] and Potential energy surface (c) for simultaneous rotation of C15-C18 and C8-C15 bond of psilocin molecule generated at B3LYP/cc-pVTZ level of theory. (Number after the atomic symbol represents the labeling scheme as per Figure 2.7).	50
2.6	Potential energy surface (a) for simultaneous C3-O30 and N21-C18 bond rotation and potential energy curve (b) for N21-C18 and (c) for C3-O30 bond rotation generated at B3LYP/cc-pVTZ level of theory. (Number after the atomic symbol represents the labeling scheme as per Figure 2.7).	51
2.7	Optimized structures of both the conformers (A & B) of psilocin; where, numbers after atoms represent the label of that atom in optimized geometry	52
2.8	Structure of Conformer-C and Conformer-D	52
2.9	Optimization with functionals (in the rectangle) and basis sets (in the circle)	53
2.10	(a, b and c) Potential energy curve [with respect to M6-conformer] of mescaline from scanning different dihedral angles and (d) potential energy surface by simultaneous rotation of C1-O19 and C9-C12 bond of mescaline generated at B3LYP/cc-pVTZ level of theory. (Number after the atomic symbol represents the labeling scheme as per Figure 2.12)	55
2.11	(a, b and c) Potential energy curve [with respect to M6-conformer] of mescaline from scanning different dihedral angles B3LYP/cc-pVTZ level of theory. (Number after the atomic symbol represents the labeling scheme as per Figure 2.12)	56
2.12	Optimized structures of mescaline conformers (M6 and M1) [numbers on atoms represent the label of that atom in the optimized geometry]	61
2.13	HOMO-LUMO (ΔE) gap of both the conformers (A & B) of psilocybin	63

2.14	HOMO-LUMO (ΔE) gap of both the conformers (A & B) of psilocin molecule	64
2.15	HOMO-LUMO (ΔE) gap of both the conformers (M6 & M1) of mescaline	66
2.16	Topological basin surfaces with Bond critical points (3,-1) of psilocybin at B3LYP/cc-pVTZ level for the Conformer-A and Conformer-B of psilocybin	76
2.17	Optimized structures of all the dimers of psilocin molecule at B3LYP/cc-pVTZ level of theory	79
2.18	Topological basin surface with Bond critical points (3, -1) of psilocin at B3LYP/cc-pVTZ level for Monomers (A and B conformers) and all the dimers of psilocin molecule	80
2.19	Topological basin surfaces with Bond critical points (3,-1) of mescaline at CCSD/cc-pVDZ level for the Conformer-M6 of mescaline	82
2.20(a)	Scatter plot of the reduced density gradient (RDG(r)) versus $\Omega(r)$ for M6 and M1 conformers of mescaline [where, iso-surface of RDG = 0.5]	83
2.20(b)	The visual diagram of RDG iso-surfaces for mescaline conformers (M6 and M1). Color gradient corresponds to the different types of interaction in respective conformers	84
2.21	Charge distribution plot of ESP[MK] charges for conformer-A and conformer-B ; the number after atoms represent the label of that atom shown in figure 2.2	85
2.22	Charge distribution plot of Hirshfeld charges for conformer-A and conformer-B	85
2.23	Charge distribution plot of Hirshfeld charges for conformer-A and B ; the number after atoms represent the label of that atom shown in article, figure 2.7	87
2.24	Charge distribution plot of ESP[MK] charges for conformer-M6 and conformer-M1 ; the number after atoms represent the label of that atom shown in figure 2.12	89
2.25	Charge distribution plot of Hirshfeld charges for conformer-M6 and M1 ; the number after atoms represent the label of that atom shown in article, figure 2.12	91
2.26	ESP map on optimized geometries of both the conformers (A & B) of psilocybin	92
2.27	ESP map on optimized geometries of both conformers (A and B) of psilocin molecule	92
2.28	ESP map on optimized geometries of both the conformers (M6 & M1) of mescaline	93
2.29	Calculated UV spectrum of conformer-A ($\lambda_{\max} = 266$ nm) and conformer-B ($\lambda_{\max} = 265$ nm) of psilocybin	94

3.1	Dihedral angle-relative energy curve [with respect to G'TG'1/G'TT] (a-d) of DTT at B3LYP/cc-pVTZ level of theory	114
3.2	Optimized structures of all DTT conformers (numbers on atoms represent the label of that atom in the optimized geometry) where, $\Delta E = E_{\text{conformer}} - E_{\text{G'TG'1/G'TT}}$	116
3.3	Optimized structure of Cyclic DTT, H ₂ molecule and G'TG'1 at CCSD/cc-pVDZ level of theory	117
3.4	Configurational isomers of DTT molecule optimized at CCSD/cc-pVDZ level of theory; $\Delta E = E_{\text{conformer}} - E_{\text{G'TG'1/G'TT}}$	118
3.5	Experimental IR spectrum of DTT(solid)	121
3.6	Experimental Raman spectrum of DTT(solid)	122
3.7	Topological basin surfaces with Bond critical points (3,-1) of DTT at CCSD/cc-pVDZ level	125
3.8(a)	Scatter plot of the reduced density gradient (RDG(r)) versus $\Omega(r)$ for all seven conformers of DTT [where, iso-surface of RDG = 0.5]	127
3.8(b)	The visual diagram of RDG iso-surfaces for DTT conformers. Color gradient corresponds to the different types of interaction in respective conformers	128
3.9	Charge distribution plot of ESP[MK] charges for DTT conformers; the number after atoms represent the label of that atom shown in figure 3.2	131
3.10	Charge distribution plot of Hirshfeld charges for all DTT conformers at CCSD/cc-pVDZ level of theory	133
3.11	ESP map on optimized geometries of DTT conformers at CCSD/cc-pVDZ level	133
3.12	HOMO-LUMO (ΔE) gap of all DTT conformers at CCSD/cc-pVDZ level of theory	134
3.13	Calculated UV spectrum of G'TG'1/G'TT conformer ($\lambda_{\text{max}} = 196.8$ nm) of DTT	136
4.1	Potential energy curve [a (C1-C4 bond rotation) and b (S5-C1 bond rotation) c (O8-C4 bond rotation)] and Potential energy surface (d) for simultaneous rotation of C1-C4 and S5-C1 bond of TGA generated at CCSD/cc-pVDZ level of theory. (Number after the atomic symbol represents the labeling scheme as per Figure 4.3)	146
4.2	Potential energy curve [a (C1-C4 bond rotation) and b (S5-C1 bond rotation) c (O8-C4 bond rotation)] of TGA generated at CCSD/cc-pVTZ level of theory. (Number after the atomic symbol represents the labeling scheme as per Figure 4.3)	147
4.3	Optimized structures of both the TGA monomers (GGC & GAC) at CCSD/cc-pVDZ level; where, numbers after atoms represent the label of that atom in optimized geometry	148
4.4	Optimized structure of GAT High energy conformer at CCSD/cc-pVDZ theoretical level	149

4.5	Optimized structures of both the TGA dimers (D1-D5) at CCSD/cc-pVDZ level; where, numbers after atoms represent the label of that atom in optimized geometry	151
4.6	Optimized structures of all 7 trimers (T1-T7) of TGA at CCSD/cc-pVDZ level; where, numbers after atoms represent the label of that atom in optimized geometry	152
4.7	Topological basin surfaces with Bond critical points (3, -1) of TGA at CCSD/cc-pVDZ level for all the dimers(D1-D5) of TGA	162
4.8	The visual diagram of RDG iso-surfaces for TGA dimers (D1-D5). Color gradient corresponds to the different types of interaction in respective clusters (dimers and trimers)	163
4.9	Topological basin surfaces with Bond critical points (3, -1) of TGA at CCSD/cc-pVDZ level for all the trimers (T1-T7) of TGA	164
4.10	The visual diagram of RDG iso-surfaces for TGA trimers (T1-T7)	165
4.11	Charge distribution plot of ESP[MK] charges for TGA monomers (GGC and GAC) [a], dimers (D1-D5) [b] and trimers(T1-T7) [c] and comparison among GGC, D1 and T1[d]; the number after atoms represent the label of that atom	175
4.12	ESP map on optimized geometries of TGA monomers, dimers and trimers at CCSD/cc-pVDZ level of theory	178
4.13	FMO iso-surface of TGA (a) monomers (GAC), (b) dimers (D2-D5) and (c) trimers (T2-T7) at CCSD/cc-pVDZ level of theory	180-181
5.1	Optimized structures at B3LYP/LANL2DZ/6-311+ +G(d,p) level of theory: 1 Cu ₉ cluster, 2 cystine, 3 Cys-Cu(A) with interaction energy (IE)= -88.34 kcal/mol, 4 Cys-Cu(B) with IE= -40.28 kcal mol, 5 Cys-Cu(C) with IE= -23.84 kcal/mol, and 6 Cys-Cu(D) with IE= -19.51 kcal/mol [atoms in Cys-Cu ₉ are numbered]	197
5.2	Interaction energy in kcal/mol at B3LYP functional but different basis sets	198
5.3	Calculated Raman Spectrum; (a) cystine and (b) Cys-Cu(A) system	199
5.4	Total density of plot of (a) Cu ₉ cluster (b) Cystine and (c) Cys-Cu(A) system showing energy of HOMO, LUMO and band gap (ΔE)	202
5.5	Topological basin surfaces with Bond critical points (3,-1) of Cys-Cu(A) system at B3LYP/LANL2DZ/6-311++G(d,p) level	204
5.6	Figure 5.6: HOMO-LUMO (ΔE) gap of (a) cystine (b) Cys-Cu(A) system	205
5.7	ESP charge density shown by colour (1) Cu ₉ , (2) cystine and (3) Cys-Cu(A) system	207
5.8	ESP Map on Cys-Cu(A) system	208
6.1	Optimized structure of (a) PATP-Cu ₅ and (b) Cu ₅ -DMAB-Cu ₅ systems at PW91PW91/LANL2DZ/6-311+G(d,p) level of theory	217
6.2	Simulated SERS spectrum of (a) PATP-Cu ₅ and (b) Cu ₅ -DMABCu ₅ system	219

6.3	Molecular orbital plots of PATP and DMAB adsorbed on copper cluster involved in photon-driven CT processes	222
6.4	Optimized structures; (a) PATP, (b) BOC cluster and (c) PATP-BOC system [the numbers after atom represent the label of respective atom]	223
6.5	Frontier Molecular Orbital diagrams of: (a) HOMO-LUMO of PATP (b) HOMO-LUMO of PATP-BOC system and (c) HOMO-LUMO of BOC cluster	224
6.6	TDOS plot for (a) PATP-Cu ₅ and (b) Cu ₅ -DMAB-Cu ₅ systems at PW91PW91/LANL2DZ/6-311+G(d,p) level of theory	226
6.7	Total density of plot of (a) BOC (Bismuthoxycarbonate) cluster (b) PATP and (c) PATP-BOC system showing energy of HOMO, LUMO and band gap (ΔE)	227
6.8	ESP map on optimized structures of (a) PATP-Cu ₅ and (b) Cu ₅ -DMAB-Cu ₅	228
A1	Optimized structure of Ba(CO) ⁺ , Ba(CO) ⁻ , Ba(CO) ₂ and Ca(CO) ₂ complexes	240

LIST OF TABLES

Table No.	DESCRIPTION	Page No.
2.1	Conformational abundance of the psilocybin molecule at B3LYP/cc-pVTZ level of theory	48
2.2	Conformational abundance of the mescaline at B3LYP/cc-pVTZ level of theory	57
2.3	Optimized geometrical parameters of both conformers A & B at B3LYP/cc-pVTZ level of theory	58
2.4	Optimized geometrical parameters of conformers A and B at B3LYP/cc-pVTZ level of theory	59-60
2.5	Optimized geometrical parameters of both conformers M6 & M1 at CCSD/cc-pVDZ level of theory	61-62
2.6	Computed energy [eV] parameters of both the conformers (A & B) of Psilocybin at B3LYP/cc-PVTZ level of theory	63
2.7	Computed energy [eV] parameters of conformers (A & B) of Psilocin molecule at B3LYP/cc-PVTZ level of theory	65
2.8	Computed energy [eV] parameters of both the conformers of mescaline at B3LYP/cc-PVTZ//CCSD/cc-pVDZ level of theory	66
2.9	Some significant donor - acceptor NBO interactions in psilocybin with calculated second order stabilization energies E(2) kcal/mol	68-69
2.10	Some significant donor - acceptor NBO interactions in psilocin molecule with calculated second order stabilization energies E(2) kcal/mol	70-71
2.11	Some significant donor - acceptor NBO interactions in mescaline with calculated second order stabilization energies E(2) kcal/mol at CCSD/cc-pVDZ level	72-74
2.12	Topological parameters for bonds of interacting atoms in psilocybin: electron density (ρ BCP), kinetic electron energy density (GBCP), potential electron energy density (VBCP), total electron energy density (HBCP), Laplacian of electron density (∇^2 BCP), estimated interaction energy (Eint) at bond critical point (BCP)	75
2.13	BSSE Corrected Interaction energy of all the dimers of Psilocin at B3LYP/cc-pVTZ level of theory	78
2.14	Topological parameters for bonds of interacting atoms in psilocin (for monomers and dimers): electron density (ρ BCP), kinetic electron energy density (GBCP), potential electron energy density (VBCP), total electron energy density (HBCP), Laplacian of electron density (∇^2 BCP), estimated interaction energy (Eint) at bond critical point (BCP)	81-82
2.15	The Hirshfeld and ESP[MK] charge values [a.u.] on each atom of both the conformers (A & B) of psilocybin molecule	86

2.16	The Hirshfeld charge values (a.u.) on each atom of both the conformers (A & B) of psilocin molecule	88
2.17	The ESP[MK] and Hirshfeld charge values (a.u.) on each atom of both the conformers (M6 & M1) of mescaline at CCSD/cc-pVDZ level of theory at CCSD/cc-pVDZ level of theory	90
2.18	Comparison of experimental and simulated ¹ H NMR peaks of psilocybin at B3LYP/cc-pVTZ level of theory	94
2.19	Calculated and experimental IR vibrational frequencies of psilocybin at B3LYP/cc-pVTZ level of theory	95
2.20	Comparison of experimental and simulated ¹ H-NMR peaks of psilocin at B3LYP/cc-pVTZ level of theory	96
2.21	Calculated and experimental IR vibrational frequencies of psilocin molecule at B3LYP/cc-pVTZ level of theory	96-97
2.22	Comparison of experimental and simulated ¹ H-NMR peaks of mescaline at B3LYP/cc-pVTZ/CCSD/cc-pVDZ level of theory	98
2.23	Calculated and experimental IR vibrational frequencies of mescaline at B3LYP/cc-pVTZ//CCSD/cc-pVDZ level of theory	98
3.1	Conformational abundance of the DTT (Dithiothreitol) conformers at B3LYP/cc-pVTZ level of theory	115
3.2	Relative single point energy of all DTT conformers with respect to G'TG'1/ G'TT at CCSD(T)/CBS limit with cc-pVNZ (N=T,Q)	117
3.3	Optimized bond lengths in all DTT conformers and arsenite complex [As- G'TG'1/ G'TT] at CCSD/cc-pVDZ level of theory	118-119
3.4	Optimized bond angles in all DTT conformers and arsenite complex [As- G'TG'1/ G'TT] at CCSD/cc-pVDZ level of theory	119-120
3.5	Relative change in Thermodynamic parameters of all DTT conformers with respect to G'TG'1/ G'TT conformer at CCSD/cc-pVDZ level of theory	120
3.6	Comparison of experimentally observed IR/Raman active vibrational modes with the calculated IR/Raman active modes in G'TG'1 conformer of DTT at B3LYP/cc-pVTZ//CCSD/cc-pVDZ level of theory	1222-123
3.7	Hydrogen-bond parameters for all DTT conformers at CCSD/cc-pVDZ level	124
3.8	Topological parameters for bonds of interacting atoms in DTT: electron density (ρ BCP), kinetic electron energy density (GBCP), potential electron energy density (VBCP), total electron energy density (HBCP), Laplacian of electron density (∇^2 BCP), estimated interaction energy (E _{int}) at bond critical point (BCP)	125
3.9	Some significant donor - acceptor NBO interactions in DTT molecule with calculated second order stabilization energies E(2) kcal/mol	129-130
3.10	The ESP[MK] charge values [a.u.] on each atom of DTT	131-132

	conformers at CCSD/cc-pVDZ level of theory	
3.11	The Hirshfeld charge values [a.u.] on each atom of DTT conformers at CCSD/cc-pVDZ level of theory	132
3.12	Computed energy [eV] parameters of all DTT conformers at CCSD/cc-pVDZ level of theory	135
3.13	Comparison of experimental and simulated ¹ H NMR peaks of DTT Conformer (G'TG'1/G'TT)	137
4.1	Relative single point energy difference (CBS limit) with respect to GGC conformer (kcal/mol) at CCSD(T)/ (cc-pVNZ, N=T, Q) level	149
4.2	Calculated Interaction Energy of TGA(GGC) Dimers at CCSD/cc-PVDZ level of theory	151
4.3	Calculated Interaction Energy of TGA(GGC) Trimers at CCSD/cc-PVDZ level of theory	153
4.4a	Optimized geometries, rotational constants (MHz) [A, B, C], inertia defect (amu. Å ² [ΔC] of TGA monomers (GGC and GAC) at CCSD/cc-pVDZ level of theory (R is distance in Å, Θ is angle in degree (°)	153
4.4b	Optimized geometrical parameters of dimers of TGA at CCSD/cc-pVDZ (R is distance in Å, Θ is angle in degree (°)	154-155
4.4c	Optimized geometrical parameters of trimers of TGA at CCSD/cc-pVDZ (R is distance in Å, Θ is angle in degree (°)	155-157
4.5	Comparison of interaction energy [§] (kcal/mol) and bond length for Relative Single point relative energy difference (CBS limit) with respect to D1 dimer (kcal/mol) at CCSD(T)/cc-pVNZ (N=T, Q) level	158
4.6	Calculated ZPE (zero-point energy) + BSSE corrected and only BSSE corrected Interaction energy (kcal/mol) for dimers and trimers clusters of TGA	158
4.7	DLPNO-CCSD(T) based Local Energy Decomposition (LED) of energy terms for the TGA(GGC) Dimers and Trimers	160
4.8	Topological parameters for bonds of interacting atoms in TGA Dimers and Trimers: electron density (ρBCP), kinetic electron energy density (GBCP), potential electron energy density (VBCP), total electron energy density (HBCP), Laplacian of electron density (∇ ² ρBCP), estimated interaction energy (E _{int}) at bond critical point (BCP)	166-167
4.9a	Some significant donor - acceptor NBO interactions in TGA monomers (GGC and GAC) with calculated second order stabilization energies E (2) kcal/mol at CCSD/cc-pVDZ level	169-170
4.9b	Some significant donor - acceptor NBO interactions in TGA dimers (D1-D5) with calculated second order stabilization energies E (2) kcal/mol at CCSD/cc-pVDZ level	170-171
4.9c	Some significant donor - acceptor NBO interactions in TGA trimers	171-173

	(T1-T7) with calculated second order stabilization energies E (2) kcal/mol at CCSD/cc-pVDZ level	
4.10a	The ESP[MK] charge values [a.u.] on each atom of both the conformers (GGC & GAC) of TGA at CCSD/cc-pVDZ level of theory	175
4.10b	The ESP[MK] charge values [a.u.] on each atom of all dimers (D1-D5) clusters of TGA at CCSD/cc-pVDZ level of theory	176
4.10c	The ESP[MK] charge values [a.u.] on each atom of all trimers (T1-T7) clusters of TGA at CCSD/cc-pVDZ level of theory	176-177
4.11	Computed energy (eV) parameters of TGA monomers, dimers and trimers at CCSD/cc-PVDZ level of theory	179
4.12	Calculated and experimental selective IR vibrational modes of TGA monomer (GGC), dimers (D1-D5) and trimers (T1-T7) at B3LYP/cc-pVTZ//CCSD/cc-pVDZ level of theory	183-184
4.13a	Calculated IR vibrational modes of TGA monomers (GGC & GAC) at B3LYP/cc-pVTZ//CCSD/cc-pVDZ level of theory	184
4.13b	Calculated IR vibrational modes (cm-1) of TGA dimers (D1-D5) at B3LYP/cc-pVTZ//CCSD/cc-pVDZ level of theory	184-185
4.13c	Calculated IR vibrational modes (cm-1) of TGA trimers (T1-T7) at B3LYP/cc-pVTZ//CCSD/cc-pVDZ level of theory	185
5.1	Calculated and Experimental Raman active normal modes of vibrations of cystine at B3LYP/LANL2DZ/6-311++G(d,p) level of theory	199
5.2	Calculated bond length (Å) of Cys-Cu(A) system at B3LYP/LANL2DZ/6-311++G(d,p) level of theory	201
5.3	Some significant donor-acceptor NBO interactions in Cys-Cu(A) system with calculated second-order stabilization energies E(2) (kcal/mol)	203
5.4	Topological parameters for bonds of interacting atoms in Cys-Cu(A) system: electron density (ρ_{BCP}), kinetic electron energy density (GBCP), potential electron energy density (VBCP), total electron energy density (HBCP), Laplacian of electron density ($\nabla^2 BCP$), estimated interaction energy (Eint) at bond critical point (BCP)	204
5.5	Computed energy [eV] parameters at B3LYP/cc-PVTZ level of theory	206
5.6	Results of MK[ESP] charge calculation at B3LYp/LANL2DZ/6-311++G(d,p) level of theory	207
6.1	Comparison of Raman spectrum of PATP before and after adsorption on Cu ₅ cluster with Experimental Raman spectrum of solid PATP from literature	217
6.2	Comparison of Simulated SERS of PATP@Cu with previously reported Simulated SERS of PATP@Ag and PATP@Au	218

6.3	Comparison of Experimentally observed SERS of PATP@Cu with simulated Raman (DMAB) and SERS of Cu ₅ -DMAB-Cu ₅ at PW91PW91/LANL2DZ/6-311+G(d,p) level of theory	218-219
6.4	Comparison of the calculated and experimental SERS vibrational frequencies of PATP on the BOC cluster at the PW91PW91/LANL2DZ/ 6-311+G(d,p) level of theory	223
6.5	MK[ESP] charge values (a.u.) calculated for Cu ₅ -DMAB-Cu ₅ and PATP-Cu ₅ system at PW91PW91/LANL2DZ/6-311+G(d,p) level of theory	229
A1	Comparison of calculated CO stretching vibrational frequency with experimentally reported frequency in alkaline earth metal carbonyl complexes [Ba(CO) ⁺ , Ba(CO) ⁻ and Ba(CO) ₂]	241
A2	Comparison of calculated CO stretching vibrational frequency with experimentally reported frequency in alkaline earth metal carbonyl complexes [Ca(CO) ₂]	242

PREFACE

The quantum chemical computations were conducted to explore conformations of few organic molecules and to study the interaction using different methods like DFT, MP2 and CCSD with different basis sets. Gaussian 16 suit of program, Orca 5.0 and Multiwfn were utilized to perform these calculations. The following paragraphs present the summary of each chapter.

Chapter 1 serves as an introduction to conformational analysis and non-covalent interactions, exploring their diverse aspects. The non-covalent interactions were explored, encompassing their nature and strength. An array of spectroscopic details that could be computed gets introduced which are helpful in gaining insight on the conformation and non-covalent interactions. Furthermore, the effectiveness of DFT calculations in understanding the interaction between metal clusters and molecules was discussed. The chapter further provides comprehensive information on quantum chemical methods, basis sets, and computational tools employed to infer diverse molecular properties. Finally, the chapter was concluded by outlining the objectives of the work entailed in this thesis.

Chapter 2 focuses on the conformational analysis of three psychedelic molecules namely psilocybin, psilocin, and mescaline. Each molecule exhibited distinct conformers, including the global minimum conformer. These conformers demonstrated various intramolecular H-bonding interactions and other NC-interactions, contributing to the stability of the global minimum. These interactions were studied through AIM, NCI and NBO calculations. Relaxed dihedral scans were performed utilizing the B3LYP/cc-pVTZ level of theory. Psilocybin exhibited the existence of two stable conformers. The energy difference between global minimum and second most stable conformer was found to be 2.08 kcal/mol with a rotational barrier of 14.6 kcal/mol between them. Similarly, psilocin also exhibited two stable conformers, with an energy difference of 5.4 kcal/mol between the local and global minimum. Notably, these conformers displayed different intramolecular hydrogen bonding patterns. Conformer-A of psilocin exhibited a strong intramolecular H-bond between the indolic hydroxy group and ethyl amine, whereas Conformer-B lacked this interaction. To further understand the strength of intra- versus intermolecular H-bonding, we studied dimers of both conformers of psilocin. The dimers of Conformer-A displayed a stronger intramolecular H-bond compared to the intermolecular H-bond, while the reverse was observed in Conformer-B. Another psychedelic molecule namely mescaline was investigated. Two equally populated low-energy conformers differing by approximately 0.5 kcal/mol and 1.5 kcal/mol at the

B3LYP/cc-pVTZ and CCSD/cc-pVDZ levels of theory, respectively, were identified. These conformers varied in the orientation of the alkylamine group relative to the benzene ring, mediated by the NH... π interaction. The geometrical parameters of these conformers aligned well with a previously reported X-ray crystal structure study. Furthermore, our spectroscopic analysis, including ¹H-NMR, UV, and vibrational mode calculations, exhibited agreement with literature data for all three molecules (psilocybin, psilocin, and mescaline).

Chapter 3 encompasses an extensive exploration of the conformational landscape of dithiothreitol (DTT), resulting in the identification of seven minimum energy geometries. This investigation involved varying the prominent dihedral angles in the molecule through a relaxed scan, with a step size of 5°, initially carried out at the B3LYP/cc-pVTZ theoretical level. Further geometry optimization was conducted at the CCSD/cc-pVDZ theoretical level. And at the CCSD(T)/CBS limit with the cc-pVNZ (N=T,Q) level of theory, single point energies were also calculated for all conformers which consistently revealed similar energy patterns. Among the conformers, two iso-energetic structures, namely G'TG'1 and G'TT, were identified, despite their significant structural differences. These two conformers exhibited the lowest energy compared to the others. In contrast, the cyclic and other configurational counterparts of the global minimum had a considerable higher energy. An intriguing observation was the stabilization of the global minimum structure of DTT through an intramolecular sulfur-centered hydrogen bond. This was established through various analyses, including AIM, NBO, FMO, and ESP charge analysis. Furthermore, the computed harmonic normal modes and NMR (Nuclear Magnetic Resonance) spectra of DTT matched appreciably with the available and observed experimental data.

In Chapter 4, the conformational landscape of thioglycolic acid (TGA) was examined using the CCSD/cc-pVDZ theoretical level. The GGC conformer was identified as the global minimum with the GAC conformer following closely. The rotational constant calculated for the GGC conformer exhibited good concordance with the earlier reported experimental findings. Furthermore, the study explored sulfur-centered hydrogen bonding in TGA's dimer and trimer clusters, employing the CCSD/cc-pVDZ theoretical level where it was seen that both oxygen and sulfur atoms were equally involved in the non-covalent H-bonding contributing to the stability. The presence of these non-covalent interactions in TGA clusters were further elucidated through AIM, RDG, and NBO analysis. Additionally, ESP charge and vibrational mode analysis provided further support for these findings.

In Chapter 5, an exploration into the stability of the disulfide bond within cystine on a copper cluster (Cu₉) was undertaken. This investigation utilized the B3LYP/LAN-L2DZ/6-

311++G(d,p) level of theory. The geometries of unconnected cystine and Cu₉ were optimized individually and the resulting geometry was used as an input. The outcomes indicated that cystine adhered to Cu₉ primarily through its disulfide and carboxyl functional groups. The simulation of the Raman spectrum revealed the disruption of the disulfide linkage, marked by the absence of the -S-S- stretching mode, aligning with prior experimental observations. Furthermore, the NBO results unveiled the contribution of lone pairs of electrons from oxygen and sulfur atoms to copper in the Cu₉-cystine system. Moreover, the outcomes derived from MK ESP charge, FMO, and AIM calculations supported the aforementioned findings.

In Chapter 6, the chemical transformation of PATP to its dimer DMAB (p,p-dimercaptoazobenzene) on copper nanoclusters and its stability on bismuth-based cluster i.e. the BOC (bismuthoxycarbonate) cluster, are discussed. For this study the generalized gradient approximation for exchange-correlation functionals PW91PW91 was employed. For the copper and bismuth atoms, relativistic effective core potentials (RECP) using LANL2DZ were used, whereas the C, H, N, S, and O atoms were studied using the 6-311++G(d,p) basis set. The SERS spectrum of DMAB on copper clusters, as simulated, was significantly similar to the SERS spectrum of PATP on copper observed in experiment. In contrast, the SERS spectrum simulated for PATP-BOC exhibited notable agreement with the corresponding experimental SERS spectrum, showing no dimerization. The dimerization of PATP on copper clusters was associated with metal-to-molecule charge transfer, while the authentic SERS spectrum of PATP was derived from molecule-to-metal charge transfer when the BOC cluster was employed as the SERS substrate.

Appendix: It includes the calculation of vibrational frequencies for Ba(CO)_n and Ca(CO)_n systems, where n=1, and 2. The main objective is to support experimental vibrational results by employing various combinations of basis sets in ab initio and DFT methods. A noteworthy investigation conducted by Xuan et al., revealed the existence of a novel covalent bond between CO and alkaline earth metals such as Ba, Ca, and Sr. However, there was a considerable disparity between their experimentally determined vibrational frequencies and the frequencies calculated theoretically. Our aim was to identify an appropriate method for accurately calculating the vibrational frequencies of alkaline earth metal complexes. To achieve this, we employed several ab initio and DFT methods, along with varying combinations of basis sets.